The Astrophysical Journal, 628:789–799, 2005 August 1
© 2005. The American Astronomical Society. All rights reserved. Printed in U.S.A.

HIGH-RESOLUTION MOLECULAR LINE OBSERVATIONS OF THE ENVIRONMENT OF THE CLASS 0 SOURCE B1-IRS

Itziar de Gregorio-Monsalvo,[1,2] Claire J. Chandler,[2] José F. Gómez,[1] Thomas B. H. Kuiper,[3] José M. Torrelles,[4] and Guillem Anglada[5]

Received 2004 December 1; accepted 2005 April 6

ABSTRACT

In this work we present VLA observations of the NH_3, CCS, and H_2O maser emission at 1 cm from the star-forming region B1-IRS (IRAS 03301+3057) with $\simeq 5''$ (=1750 AU) of angular resolution. The CCS emission is distributed in three clumps around the central source. These clumps exhibit a velocity gradient from red- to blueshifted velocities toward B1-IRS, probably due to an interaction with the outflow from an embedded protostar. The outflow and its powering source are traced by a reflection nebula and an associated infrared point source detected in a 2MASS *K*-band image. We find that this infrared point source is associated with water maser emission distributed in an elongated structure ($\simeq$450 AU) along the major axis of the reflection nebula and tracing the base of the outflow of the region. Ammonia emission is extended and is spatially anticorrelated with CCS. This is the first time that this kind of anticorrelation is observed in a star-forming region with such a high angular resolution, and it illustrates the importance of time-dependent chemistry on small spatial scales. The relatively large abundance of CCS with respect to ammonia, compared with that in other star-forming regions, suggests an extreme youth for the B1-IRS object ($\leq 10^5$ yr). We suggest the possibility that CCS abundance is enhanced via shock-induced chemistry.

Subject headings: ISM: individual (B1-IRS) — ISM: jets and outflows — ISM: kinematics and dynamics — ISM: molecules — stars: formation — stars: pre–main-sequence

1. INTRODUCTION

The spatial distribution of emission from various molecular tracers in star-forming clouds depends not only on the physical conditions within the clouds, but also on the (time dependent) chemistry. This is very clearly the case for CCS and NH_3, where a pronounced spatial anticorrelation in the emission from these two species has been reported for quiescent, starless cores (Suzuki et al. 1992). A spatial anticorrelation has also been observed on large-scale maps in several individual sources, such as TMC-1 (Hirahara et al. 1992), L1498 (Kuiper et al. 1996), and B68 (Lai et al. 2003).

The lines of CCS are very appropriate for studying the structure and the physical conditions in dark clouds because they are not very opaque (Saito et al. 1987), and yet they are intense and abundant (Suzuki et al. 1992). Its lack of hyperfine splitting and the fact that it is heavier than other high-density tracers (thus showing intrinsically narrower lines) make CCS a very well suited molecule for carrying out dynamical studies. NH_3 emission tends to trace the inner, denser regions of molecular cores, while CCS shows up slightly outside these central regions with a clumpy distribution (Suzuki et al. 1992). This relative distribution has been explained in terms of chemical and dynamical evolution of the protostellar core: CCS lines are intense in cold quiescent cores, but when the cloud evolves and star formation begins, high-velocity outflows and radiation from protostars destroy carbon chain molecules. At the same time, these conditions favor the desorption of NH_3 from dust grains. For this reason, the abundance ratio [CCS]/[NH_3] has been considered an indicator of evolution in protostellar cores (Suzuki et al. 1992).

CCS is rarely found to be associated with evolved star-forming regions. On the other hand, emission from both CCS and NH_3 has been detected from the Class 0 protostar B335 (Menten et al. 1983; Velusamy et al. 1995), suggesting that a combination of both molecules can be used as a means of identifying the youngest protostars and of studying their environments over a range of physical and chemical regimes. Class 0 protostars have been proposed to be in the earliest stages of low-mass stellar evolution (André et al. 1993). Processes related to mass-loss phenomena occur prominently during this phase: collimated jets, powerful molecular outflows, and protoplanetary disks of hundreds of AUs are commonly detected in this kind of source (Chandler & Sargent 1993; Terebey et al. 1993). CCS and NH_3 may therefore trace the interaction of these phenomena with the surrounding environment, providing information about the kinematics, temperature, and density in the close vicinity of very young stellar objects (YSOs).

Water maser emission has also been shown to be a good tracer of mass-loss activity in YSOs (Rodríguez et al. 1980; De Buizer et al. 2005). Previous studies suggest that water maser emission provides a good characterization of the age of low-mass YSOs, with Class 0 sources being the most probable candidates to harbor water masers (Furuya et al. 2001). Water masers have been detected in both circumstellar disks and outflows. This dichotomy has also been suggested to be a time-dependent effect, with masers tracing disks in younger objects and tracing outflows in somewhat more evolved sources (Torrelles et al. 2002).

[1] Laboratorio de Astrofísica Espacial y Física Fundamental (LAEFF-INTA), Apartado 50727, E-28080 Madrid, Spain.
[2] National Radio Astronomy Observatory (NRAO), P.O. Box O, Socorro, NM 87801.
[3] Jet Propulsion Laboratory, California Institute of Technology, Pasadena, CA 99109.
[4] Instituto de Ciencias del Espacio, CSIC; and Institut d'Estudis Espacials de Catalunya, Edifici Nexus, Gran Capità 2-4, E-08034 Barcelona, Spain. On sabbatical leave at the UK Astronomy Technology Center, Royal Observatory, Edinburgh, Blackford Hill, Edinburgh EH9 3HJ, UK.
[5] Instituto de Astrofísica de Andalucía, CSIC, Apartado 3004, E-18080 Granada, Spain.

The far-infrared source B1-IRS (IRAS 03301+3057) is one of the few sources known to exhibit both CCS and water maser emission in the studies by Suzuki et al. (1992) and Furuya et al. (2001). This is a Class 0 source (Hirano et al. 1997) located in the Perseus OB2 complex at a distance of 350 pc (Bachiller et al. 1990). The B1 cloud contains a large amount of molecular gas, as shown by the strong $C^{18}O$ (1–0) emission detected by Bachiller & Cernicharo (1984). There is no optically visible counterpart of B1-IRS, but 850 μm dust continuum emission has been detected by Matthews & Wilson (2002) using the Submillimeter Common-User Bolometric Array (SCUBA). There are two compact SiO clumps in the vicinity of B1-IRS (Yamamoto et al. 1992), and blueshifted CO (1–0) emission was observed by Hirano et al. (1997), who suggested the presence of a pole-on molecular outflow. The SiO clumps are located at the interface between the CO outflow and the dense gas traced by the $C^{18}O$, suggesting that the outflow, probably driven by the *IRAS* source, is interacting with the surrounding medium, thus yielding the SiO emission through shocks.

In this work, we have used the Very Large Array (VLA) of the National Radio Astronomy Observatory (NRAO)[6] to study the properties of the CCS, NH_3, and water maser emission from B1-IRS in order to obtain information about its circumstellar dynamics and its stage of evolution. The rest frequencies of the CCS and H_2O transitions are sufficiently close together that they can be observed simultaneously with the VLA, also offering the possibility of using the water masers to track tropospheric phase fluctuations, if the masers are strong enough. Unfortunately, this was not the case at the time of the observations presented here, but the atmosphere was in any case very stable.

This paper is structured as follows. In § 2 we describe our observations and data reduction procedure, as well as the analysis of VLA archive data. In § 3 we present our observational results (morphology and physical parameters), which are then discussed in § 4. We summarize our conclusions in § 5.

2. OBSERVATIONS AND DATA PROCESSING

Simultaneous observations of the $J_N = 2_1 - 1_0$ transition of CCS (with a rest frequency of 22344.033 MHz) and the $6_{16}-5_{23}$ transition of H_2O (with a rest frequency of 22235.080 MHz) were carried out on 2003 April 4 using the VLA in its D configuration. The phase center of these observations was R.A. = $03^h33^m16^s.3$, decl. = $31^\circ07'51''$ (J2000.0). We used the four intermediate frequency (IF) spectral-line mode, with two IFs for each molecular transition, one in each of the right and left circular polarizations. For the CCS observations we sampled 128 channels over a bandwidth of 0.781 MHz centered at V_{LSR} = 6.8 km s^{-1}, with a velocity resolution of 0.082 km s^{-1}. Water maser observations were obtained using 64 channels over a 3.125 MHz bandwidth centered at V_{LSR} = 15.7 km s^{-1}, with 0.66 km s^{-1} velocity resolution. The total on-source integration time was $\simeq$7.5 hr. Our primary calibrator was 3C 48, for which we adopted a flux density of 1.1253 Jy (at the CCS frequency) and 1.1315 Jy (at the H_2O frequency) using the latest VLA values (1999.2). The source 3C 84 was used as a phase and bandpass calibrator (with a bootstrapped flux density of 11.80 $\pm$ 0.14 Jy at the CCS frequency and 11.65 $\pm$ 0.14 Jy at the H_2O frequency). Calibration and data reduction were performed with the Astronomical Image Processing System (AIPS) of the NRAO.

[6] The NRAO is operated by Associated Universities, Inc., under cooperative agreement with the National Science Foundation (NSF).

CCS data were reduced applying spectral Hanning smoothing and natural weighting of the visibilities to improve the signal-to-noise ratio. The final velocity resolution is 0.16 km s^{-1}, and the synthesized beam is $4''.33 \times 3''.30$ (P.A. = $-79^\circ.2$). Water maser maps were produced using a "robust" weighting (Briggs 1995) of 0 to optimize a combination of both angular resolution and sensitivity. The synthesized beam obtained is $3''.29 \times 2''.73$ (P.A. = $87^\circ.9$).

In order to compare our water maser results with those at other epochs, we also retrieved earlier H_2O data from the VLA archive. These observations were carried out on 1998 October 24 and 1999 February 26, in the CnB and CD configurations, respectively, for project AF354. These data have been published by Furuya et al. (2003). Both sets of observations were made in the one IF spectral-line mode, in right circular polarization only, with a bandwidth of 3.125 MHz centered at V_{LSR} = 0 km s^{-1}, and sampled over 128 channels, thus providing a velocity resolution of 0.33 km s^{-1}. The phase center of these observations was R.A. = $03^h33^m16^s.030$, decl. = $31^\circ07'34''.05$ (J2000.0). The time on source was $\simeq$3 minutes in 1998 and $\simeq$13 minutes in 1999. In both epochs 3C 48 was used as the primary flux calibrator, with an assumed flux density of 1.1313 and 1.1315 Jy for the 1998 and 1999 observations, respectively (adopting the latest 1999.2 VLA values). The secondary calibrator was 0333+321, with a bootstrapped flux density of 1.66 $\pm$ 0.10 Jy for the 1998 observations and 1.67 $\pm$ 0.03 Jy for the 1999 observations. The water masers were strong enough during these earlier observations to enable self-calibration after referencing the maser positions to 0333+321. Images were made with the robust parameter set to 0, giving synthesized beams of $0''.91 \times 0''.38$ (P.A. = $81^\circ.7$) and $3''.05 \times 1''.16$ (P.A. = $68^\circ.8$) for the 1998 and 1999 data, respectively.

We have also processed VLA archive data of the NH_3 (1, 1) inversion transition (with a rest frequency of 23694.496 MHz). The observations were made on 1988 August 13 for project AG265, in the D configuration. The total bandwidth was 3.125 MHz, centered at V_{LSR} = 6.1 km s^{-1} and sampled by 128 channels, which provided a velocity resolution of 0.33 km s^{-1}. Both right and left circular polarizations were obtained. The phase center of these observations was R.A. = $03^h33^m16^s.337$, decl. = $31^\circ07'51''.03$ (J2000.0). The total time on source was $\simeq$2 hr. The source 3C 48 was used as the primary flux calibrator, with an adopted flux density of 1.0542 Jy (using 1999.2 values). The phase calibrator was 3C 84 (with a bootstrapped flux density of 38.0 $\pm$ 1.5 Jy). Since the NH_3 emission was faint and extended, we reduced the data using natural weights and a *u-v* taper of 20 kλ to improve the sensitivity to the extended emission. The resulting synthesized beam is $8''.62 \times 7''.76$ (P.A. = $-75^\circ.5$). The size of the VLA primary beam at the frequencies corresponding to the CCS, H_2O, and NH_3 transitions ($\simeq$22 GHz) is $\simeq 2'$.

To have an estimate of the missing flux density due to the lack of short spacings of the VLA, we have obtained single-dish spectra of both CCS and NH_3 toward the position R.A. = $03^h33^m16^s.3$, decl. = $31^\circ07'51''$ (J2000.0) with the National Aeronautics and Space Administration's (NASA's) 70 m antenna (DSS 63) at Robledo de Chavela, Spain, at the same frequencies as the VLA. This antenna has a 1.3 cm receiver composed of a cooled high electron mobility transistor (HEMT) amplifier. A noise diode is used to calibrate the data. The half-power beam width at this frequency is $\simeq 41''$, and the mean beam efficiency is $\simeq$0.4. Observations were made in frequency-switching mode, using a 256 channel autocorrelator spectrometer. The CCS observations were performed in six time slots between 2002 August and 2003 July, with a total integration time of 60 minutes and an average system temperature of $\simeq$80 K. We used a bandwidth of 1 MHz

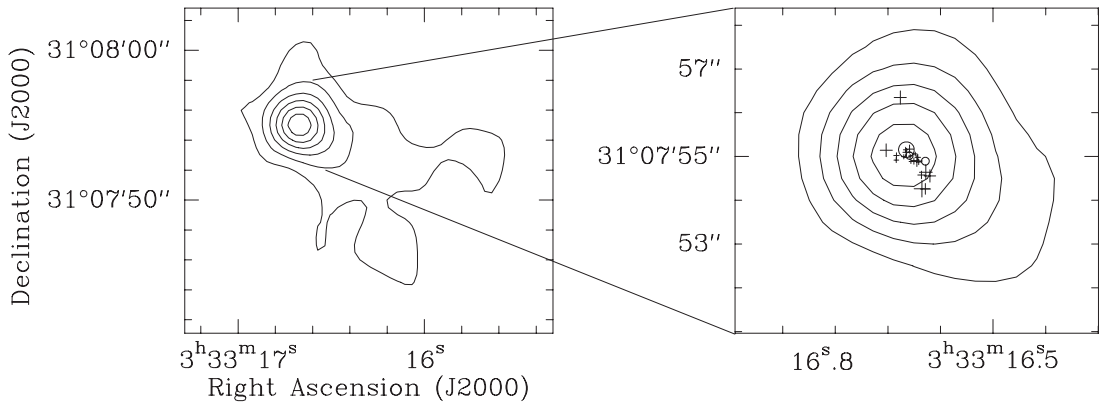


FIG. 1.—2MASS *K*-band image convolved with a 5″ Gaussian. Contours represent 90%, 75%, 60%, 45%, 30%, and 15% of the peak emission (the source magnitude is $K = 14.208 \pm 0.122$, measured by 2MASS). Plus signs and circles in the close-up of the infrared emission (*right*) represent the structure of red- and blueshifted water masers, respectively, obtained in the 2003 April observations and scaled by their relative position uncertainty.

(with a velocity resolution of 0.05 km s^{-1}). The NH_3 observations were carried out during 2003 July, with an average system temperature of $\simeq$60 K. The on-source integration time was 40 minutes. To detect all the hyperfine lines, we used a bandwidth of 10 MHz (with a velocity resolution of 0.5 km s^{-1}). The rms pointing accuracy of the telescope was better than 9″. All the single-dish data reduction was carried out using the CLASS package, developed at the Institut de Radioastronomie Millimétrique (IRAM) and the Observatoire de Grenoble as part of the GAG software.

In addition to the radio data, we have retrieved a *K*-band image from the Two Micron All Sky Survey (2MASS) to obtain a better position for the infrared source. This image was smoothed with a 5″ Gaussian (FWHM) to search for low surface brightness, extended emission.

3. RESULTS

3.1. *The Infrared Source*

The 2 μm map obtained from the 2MASS archive and convolved with a 5″ Gaussian (Fig. 1), shows a point source, designated 2MASS J03331667+3107548, at R.A. = $03^h33^m16^s.678$, decl. = 31°07′54″.88 (J2000.0) (with a 2 σ absolute position error of $\simeq$0″.22). This position is $\simeq$6″ away from the *IRAS* catalog position, R.A. = $03^h33^m16^s.3$, decl. = 31°07′51″ (J2000.0),

TABLE 1
WATER MASER COMPONENTS ON 2003 APRIL 4

R.A. (J2000.0)	Decl. (J2000.0)	Position Uncertainty[a, b] (arcsec)	Flux Density[a] (mJy)	V_{LSR}[c] (km s^{-1})
03 33 16.62.....	31 07 54.6	0.3	4.3 ± 1.6	9.1
03 33 16.629.....	31 07 54.89	0.17	7.3 ± 1.7	3.8
03 33 16.63.....	31 07 54.3	0.3	4.9 ± 1.7	19.0
03 33 16.63.....	31 07 54.6	0.3	3.9 ± 1.7	22.3
03 33 16.636.....	31 07 54.58	0.17	7.1 ± 1.7	10.4
03 33 16.64.....	31 07 54.3	0.4	3.2 ± 1.7	22.9
03 33 16.641.....	31 07 54.88	0.13	9.7 ± 1.6	14.4
03 33 16.643.....	31 07 54.98	0.13	9.3 ± 1.6	11.7
03 33 16.648.....	31 07 55.06	0.09	13.1 ± 1.6	15.0
03 33 16.650.....	31 07 54.89	0.14	8.6 ± 1.6	18.3
03 33 16.65.....	31 07 54.9	0.3	4.7 ± 1.7	16.4
03 33 16.656.....	31 07 54.88	0.09	14.7 ± 1.7	12.4
03 33 16.657.....	31 07 55.01	0.08	15.4 ± 1.6	17.7
03 33 16.659.....	31 07 55.02	0.16	7.8 ± 1.7	3.2
03 33 16.659.....	31 07 55.17	0.19	6.4 ± 1.6	11.1
03 33 16.665.....	31 07 55.09	0.17	6.9 ± 1.6	9.8
03 33 16.666.....	31 07 55.15	0.12	10.6 ± 1.6	13.7
03 33 16.670.....	31 07 54.99	0.10	12.3 ± 1.7	13.1
03 33 16.67.....	31 07 55.2	0.3	3.6 ± 1.7	2.5
03 33 16.68.....	31 07 56.3	0.3	4.0 ± 1.6	23.6
03 33 16.684.....	31 07 54.92	0.12	7.1 ± 1.7	17.0
03 33 16.684.....	31 07 55.02	0.13	9.2 ± 1.6	15.7
03 33 16.70.....	31 07 55.1	0.3	4.1 ± 1.6	19.7

NOTE.—Units of right ascension are hours, minutes, and seconds, and units of declination are degrees, arcminutes, and arcseconds.

[a] Uncertainties are 2 σ.

[b] Relative position uncertainties with respect to the phase center. The absolute position error of the phase center is $\sim$0″.28.

[c] Velocity of maser emission.

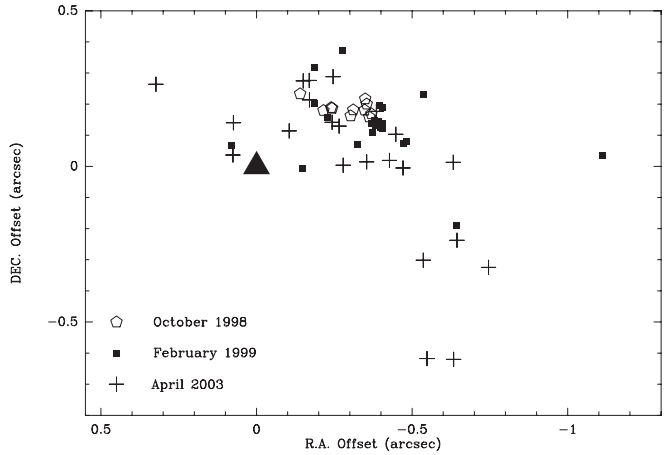


FIG. 2.—Positions of water masers observed toward B1-IRS at different epochs. Pentagons, squares, and plus signs represent the maser components observed in 1998 October, 1999 February, and 2003 April, respectively. The position offsets are relative to the 2 μm point source, which is represented by a triangle. The northernmost maser spot shown in Fig. 1 is out of the scale in this plot.

but well within the error ellipsoid (with 2 σ error axes of $48'' \times 14''$) of the latter. In what follows, we consider the position of the 2MASS point source as the location of the central source of B1-IRS. We also find extended 2 μm infrared emission elongated to the southwest of the point source, with a position angle of approximately -120°, suggestive of a reflection nebula.

3.2. *The Water Masers*

Our water maser observation in 2003 April shows a cluster of 23 maser spots (Table 1), spatially unresolved in each channel, most of which are redshifted with respect to the cloud velocity ($V_{\rm LSR} = 6.3$ km s^{-1}; Hirano et al. 1997) with local standard of rest (LSR) velocities between 9.1 and 23.6 km s^{-1}, although three are blueshifted, with LSR velocities between 2.5 and 3.8 km s^{-1}. The maximum flux density was $\simeq 15.4 \pm 1.6$ mJy at $V_{\rm LSR} = 17.7$ km s^{-1}, 2 orders of magnitude weaker than in the earlier epochs reported by Furuya et al. (2003). The masers are distributed in an elongated structure (P.A. $\simeq -120^\circ$) with a length of $\simeq 1\farcs3$ ($\simeq$455 AU).

We have compared our new data with those obtained in 1998 October and 1999 February by Furuya et al. (2003). The maser positions for those epochs are shown in Figure 2 and in Tables 2 and 3. The same elongated distribution is evident. In these earlier data sets all maser emission is redshifted with respect to the cloud velocity. We note that there is a discrepancy of $\simeq 23''$ between the positions of the 1998 October masers presented here and the positions reported in Table 3 of Furuya et al. (2003), using the same data. The positions of the masers (that we have determined by fitting two-dimensional Gaussians to the maser spots detected in each channel) are similar in all three epochs, taking into account their mean absolute positional uncertainties ($\simeq 0\farcs3$, $0\farcs16$, and $0\farcs04$ for 2003 April, 1999 February, and 1998 October, respectively). Therefore, we are confident that our positions are correct.

The water masers are located at a distance $\lesssim 1''$ (350 AU) from the 2 μm source, suggesting that this is the center of activity of the region. If we consider an average LSR velocity of $\simeq 14.0$ km s^{-1} of the maser emission, i.e., $\simeq 7.7$ km s^{-1}, redshifted with respect to the cloud velocity (6.3 km s^{-1}), and a mean distance of $0\farcs5$ from the central source, the central mass needed for the water masers to be gravitationally bound is $\simeq 12\ M_\odot$. However, B1-IRS is a low-luminosity protostar ($L \simeq 2.8\ L_\odot$; Hirano et al. 1997), and it is unlikely to be much more massive than $\simeq 1\ M_\odot$. These results strongly suggest that the masers are tracing mass-loss motions rather than bound motions in a circumstellar disk.

3.3. CCS *and* NH_3 *Emission*

3.3.1. CCS *Emission*

The integrated emission from the CCS molecule is distributed in three clumps (Fig. 3). The clump centers are located $\simeq 25''$ (9000 AU) southwest (the SW clump), $\simeq 50''$ (17,000 AU) northeast (the NE clump), and $\simeq 15''$ (5000 AU) northwest (the NW clump) from the central source. Figure 4 shows the CCS emission integrated over different velocity intervals. All clumps are redshifted with respect to the systemic velocity of the B1 core ($V_{\rm LSR} = 6.3$ km s^{-1}). Moreover, the SW, NE, and NW CCS clumps show clear velocity gradients of $\simeq 23$, $\simeq 10$, and $\simeq 12$ km s^{-1} pc^{-1}, respectively (see Figs. 5 and 6) over the whole size of the clumps,

TABLE 2
WATER MASER COMPONENTS ON 1998 OCTOBER 24

R.A. (J2000.0)	Decl. (J2000.0)	Position Uncertainty[a, b] (arcsec)	Flux Density[a] (mJy)	$V_{\rm LSR}$[c] (km s^{-1})
03 33 16.6493.....	31 07 55.049	0.024	440 ± 80	15.1
03 33 16.6498.....	31 07 55.039	0.020	570 ± 90	14.8
03 33 16.6504.....	31 07 55.080	0.017	750 ± 100	14.5
03 33 16.6509.....	31 07 55.061	0.019	560 ± 80	14.2
03 33 16.651.....	31 07 55.10	0.03	610 ± 90	13.8
03 33 16.6538.....	31 07 55.062	0.009	2300 ± 300	16.1
03 33 16.654.....	31 07 55.04	0.03	360 ± 70	13.5
03 33 16.6591.....	31 07 55.067	...[d]	2800 ± 300	15.8
03 33 16.6593.....	31 07 55.069	0.011	970 ± 130	15.5
03 33 16.661.....	31 07 55.06	0.15	1050 ± 140	16.5
03 33 16.667.....	31 07 55.11	0.07	130 ± 60	16.8

NOTE.—Units of right ascension are hours, minutes, and seconds, and units of declination are degrees, arcminutes, and arcseconds.

[a] Uncertainties are 2 σ.

[b] Relative position uncertainties with respect to the reference feature used for self-calibration.

[c] Velocity of maser emission.

[d] Reference feature. Absolute position error is $\sim 0\farcs021$.

TABLE 3
WATER MASER COMPONENTS ON 1999 FEBRUARY 25

R.A. (J2000.0)	Decl. (J2000.0)	Position Uncertainty[a, b] (arcsec)	Flux Density[a] (mJy)	V_{LSR}[c] (km s^{-1})
03 33 16.591	31 07 54.91	0.16	137 ± 23	19.1
03 33 16.628	31 07 54.69	0.14	118 ± 20	12.8
03 33 16.636	31 07 55.11	0.25	57 ± 27	20.1
03 33 16.641	31 07 54.95	0.04	352 ± 24	15.1
03 33 16.641	31 07 54.96	0.04	362 ± 21	13.2
03 33 16.646	31 07 55.00	0.05	36 ± 30	17.4
03 33 16.646	31 07 55.07	0.13	142 ± 22	18.1
03 33 16.6465	31 07 55.017	0.014	1180 ± 50	17.1
03 33 16.647	31 07 55.02	0.16	152 ± 23	18.4
03 33 16.6470	31 07 55.006	...[d]	6500 ± 230	15.8
03 33 16.6481	31 07 55.021	0.003	6010 ± 220	16.1
03 33 16.6481	31 07 55.026	0.007	2090 ± 80	15.5
03 33 16.6483	31 07 55.013	0.006	2810 ± 100	16.5
03 33 16.649	31 07 54.99	0.04	410 ± 30	13.5
03 33 16.649	31 07 55.03	0.06	236 ± 23	13.8
03 33 16.6493	31 07 55.017	0.008	1810 ± 70	16.8
03 33 16.65	31 07 55.1	0.3	45 ± 24	19.8
03 33 16.653	31 07 54.95	0.17	98 ± 23	17.8
03 33 16.660	31 07 55.04	0.10	169 ± 23	14.2
03 33 16.66	31 07 55.3	0.4	27 ± 20	11.2
03 33 16.663	31 07 55.08	0.13	17 ± 30	19.4
03 33 16.663	31 07 55.20	0.14	111 ± 22	18.8
03 33 16.666	31 07 54.87	0.11	108 ± 21	14.8
03 33 16.684	31 07 54.95	0.14	104 ± 20	14.5

NOTE.—Units of right ascension are hours, minutes, and seconds, and units of declination are degrees, arcminutes, and arcseconds.
[a] Uncertainties are 2 σ.
[b] Relative position uncertainties with respect to the reference feature used for self-calibration.
[c] Velocity of maser emission.
[d] Reference feature. Absolute position error is $\sim$0.″12.

with velocities closer to that of the ambient cloud near the central object.

The SW clump has the most redshifted velocities (V_{LSR} from 6.6 to 7.6 km s^{-1}). It has an ellipsoidal shape, elongated perpendicularly to the direction of the velocity gradient, with two emission peaks. The NE clump shows emission from $V_{LSR} = 6.6$ to 7.1 km s^{-1}, and it is divided into three "fingers" that point toward the northwest. The NW clump has a velocity gradient from $V_{LSR} = 6.3$ to 6.8 km s^{-1} (i.e., closer to the mean cloud velocity), and its morphology is elongated, with its major axis pointing toward the central source.

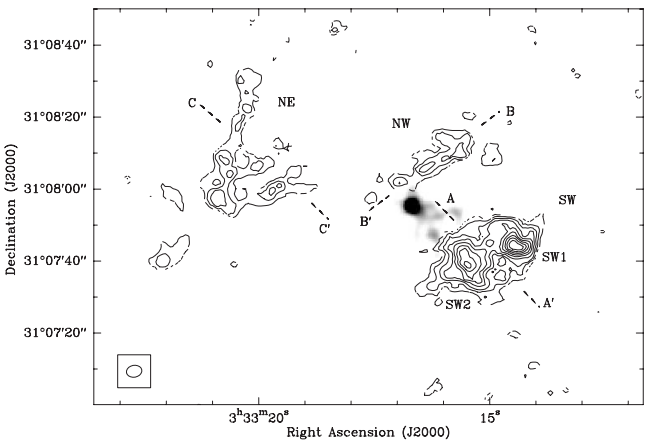


FIG. 3.—CCS integrated emission (*contours*) not corrected for the response of the VLA primary beam, overlaid on the 2MASS *K*-band emission (*gray scale*). Contour levels range from 0.66 to 5.94 mJy beam^{-1} km s^{-1} in intervals of 0.66 mJy beam^{-1} km s^{-1}. The gray scale ranges between 10% and 45% of the peak emission (the source magnitude is $K = 14.208 \pm 0.122$, measured by 2MASS). The southwest (SW), northwest (NW), and northeast (NE) CCS clumps are labeled. Dashed lines represent the axes where position-velocity diagrams have been obtained (see Fig. 6).

3.3.2. NH_3 *Emission*

Ammonia emission is very extended and clumpy (Fig. 7). Most clumps are distributed in two strips, with a northwest-southeast orientation. The general trend, however, as illustrated by Figure 7, is that CCS and NH_3 emissions are spatially anticorrelated. Such an anticorrelation has been observed in other sources (Hirahara et al. 1992; Willacy et al. 1998; Lai et al. 2003), but this is the first time that it has been detected with such a high angular resolution ($\simeq$5″).

We note, however, that there is considerable extended NH_3 (1, 1) and CCS ($J_N = 2_1$–1_0) emission in the B1-IRS region to which the VLA is not sensitive. Indeed, from our single-dish observations of these transitions (Fig. 8) we estimate that $\simeq$90% of the ammonia and CCS emission is missed by the VLA.

3.3.3. *Physical Parameters*

Although the maps shown in this paper have not been corrected by the primary beam response for display purposes, such a correction has been applied to the data prior to deriving physical parameters. Table 4 summarizes the main physical parameters obtained from the CCS and NH_3 lines. For the CCS data, we provide parameters for each individual clump, since they are well defined in the integrated intensity map (Fig. 3). For these

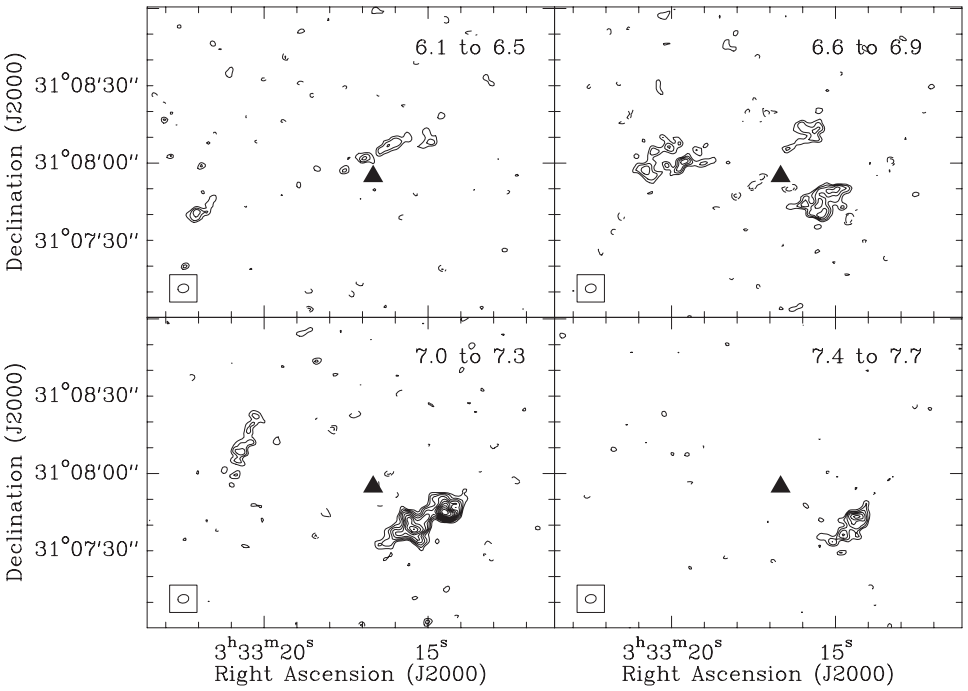


FIG. 4.—Contour maps of the CCS integrated emission over the LSR velocity ranges (in km s^{-1}) indicated in the top right corner of each panel. Contour levels are at -2.56, -1.92, and from 1.92 to 7.68 in steps of 0.64 mJy beam^{-1} km s^{-1} (the rms of the maps). The triangle indicates the 2 μm point source position. No primary beam correction has been applied to these figures.

calculations, we have divided the emission of the SW clump in two different peaks, SW1 (located at lower right ascension) and SW2 (located at the eastern part of the SW clump). The mean clump column density of CCS is $N_{\rm CCS} \simeq (3.0 \pm 0.8) \times 10^{13}$ cm^{-2}, which is similar to the value obtained by Suzuki et al. (1992) for B1 (1.38×10^{13} cm^{-2}). Assuming a relative abundance of CCS with respect to H_2 of 0.9×10^{-10} (mean value reported by Lai & Crutcher [2000] for B1), the resulting mean $N_{\rm H_2}$ is $\simeq (3.3 \pm 0.8) \times 10^{23}$ cm^{-2}.

Given the low signal-to-noise ratio and the clumpy structure of the NH_3 emission, we only give averaged values for this molecule in Table 4. The column density of ammonia at each local maximum seen in the integrated intensity map (Fig. 7) ranges between $\simeq 6 \times 10^{14}$ and 3×10^{15} cm^{-2}, with a mean clump value of $\simeq (1.4 \pm 0.4) \times 10^{15}$ cm^{-2}, similar to the value of 1×10^{15} cm^{-2} reported by Bachiller & Cernicharo (1986).

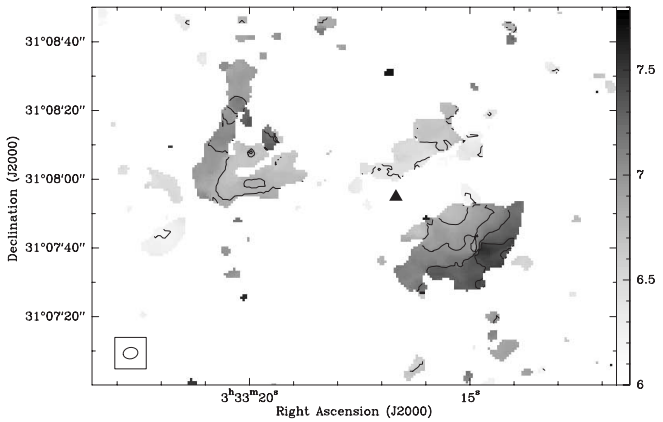


FIG. 5.—Map of CCS intensity-weighted mean velocity (first-order moment). Contour levels range from 6.0 to 7.8 km s^{-1} in steps of 0.2 km s^{-1}. The gray scale is also from 6.0 to 7.8 km s^{-1}. The triangle represents the position of the 2 μm source.

4. DISCUSSION

4.1. *The Geometry of the Molecular Outflow*

Hirano et al. (1997) detected moderately high velocity blueshifted CO emission centered close to the position of the *IRAS* source and consisting of many clumps at different blueshifted velocities. No redshifted emission was obvious in their data. Given the distribution of the blueshifted gas around the *IRAS* position (Fig. 9), Hirano et al. (1997) suggested the existence of a molecular outflow driven by the *IRAS* source and oriented pole-on with respect to the observer. In order to explain the absence of the redshifted CO lobe, these authors suggested that higher density material is slowing down that component of the outflow.

Our results, however, do not support the pole-on geometry for the outflow. The 2MASS source, which is within the error box of the *IRAS* position, is located at the tip of the blueshifted outflow rather than at its center (see Fig. 9). If we assume that the 2MASS source is actually tracing the powering source of the outflow (confirmed by its association with the water masers), its blueshifted lobe would flow toward the southwest from the central source.

The low velocity of the CO blueshifted emission with respect to the $V_{\rm LSR}$ of the cloud ($|V_{\rm CO} - V_{\rm LSR}| < 8$ km s^{-1}) and the lack of a significant amount of redshifted gas are more consistent with the molecular outflow being close to the plane of the sky. The absence of a coherent velocity gradient of the water masers along their linear structure is also consistent with this geometry.

4.2. *The Outflow Traced by Water Masers*

The water masers are distributed in the direction of the extended infrared nebula, approximately northeast-southwest. This is the same orientation as the blueshifted CO lobe with respect

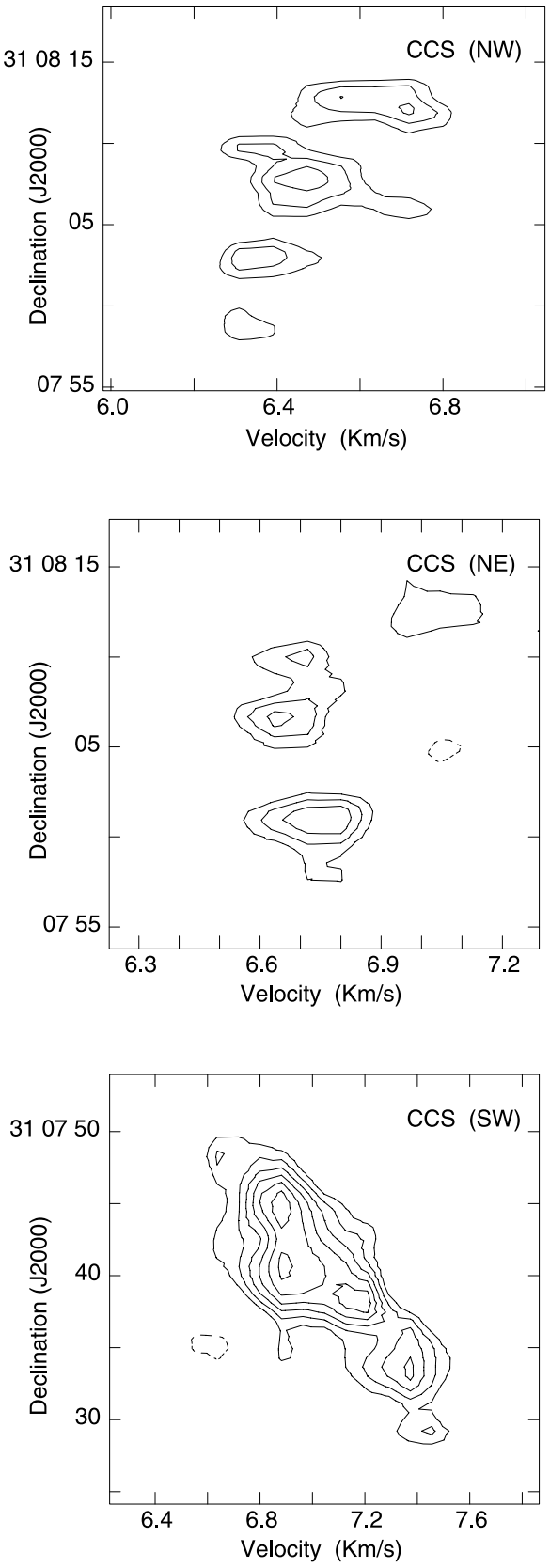


FIG. 6.—Position-velocity diagrams of the CCS clumps. *Top*, position-velocity diagram of the NW clump through axis B-B′ (see Fig. 3); *middle*, position-velocity diagram of the NE clump through axis C-C′; *bottom*, position-velocity diagram of the SW clump through axis A-A′. Contours are at −3.6 and from 3.6 to 9.6 mJy beam^{-1} in steps of 1.2 mJy beam^{-1}, the rms of the maps. These plots have not been corrected for the response of the VLA primary beam.

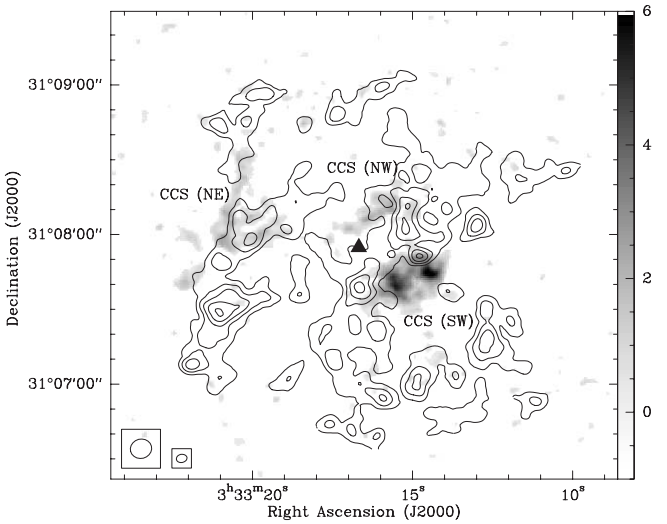


FIG. 7.—CCS (*gray scale*) and ammonia main line (*contours*) integrated emission. The gray scale ranges from −1 to 6 mJy beam^{-1} km s^{-1}. Contour levels range from 40 to 120 mJy beam^{-1} km s^{-1}, with increment steps of 20 mJy beam^{-1} km s^{-1}, the rms of the map. The triangle represents the 2 μm source. The beam on the left corresponds to the ammonia observations, and the beam on the right corresponds to the CCS observations. No primary beam correction has been applied to these maps. However, given that the phase center was almost the same in the CCS and NH_3 observations, the beam response is similar and does not affect the comparison between the two emissions.

to the central source and suggests that the masers are tracing the base of the outflow. Note, however, that most of the maser components are redshifted with respect to the cloud velocity, and yet their location primarily to the south and west of the infrared source means that they coincide with the blueshifted CO lobe. This apparent kinematic discrepancy could be explained if the masers are tracing the background walls of a cavity evacuated in the cloud by a molecular outflow close to the plane of the sky. The existence of such a cavity was suggested by Hirano et al. (1997) from their $C^{18}O$ map. In the proposed geometry of an outflow close to the plane of the sky, the background walls could show redshifted motions, assuming a finite opening angle. The fact that no corresponding blueshifted masers are shown tracing the foreground walls could be due to different physical conditions of the gas, with denser gas in the background (which probably corresponds to the region that goes deeper into the molecular cloud), and would produce a stronger interaction with the outflow in that area. Proper-motion measurements of the B1-IRS water masers will help to clarify whether our proposed geometry, with the outflow close to the plane of the sky and evacuating a cavity in the cloud, is correct.

4.3. *The Interaction between the Molecular Outflow and Its Surrounding Environment*

The CCS clumps show a clear velocity gradient, with less redshifted velocities toward the central source (see Fig. 5). If we assume that the ambient cloud velocity is 6.3 km s^{-1} (Hirano et al. 1997), these clumps would be redshifted with respect to the cloud velocity. This velocity pattern cannot be explained purely by foreground clumps with infalling motions, for which we would expect more redshifted velocities closer to the source. Nevertheless, if we consider that the CCS clumps may be interacting with the outflowing material, the infalling clumps could be slowed down closer to the central source due to this interaction, explaining in this way the less redshifted velocities at these positions.

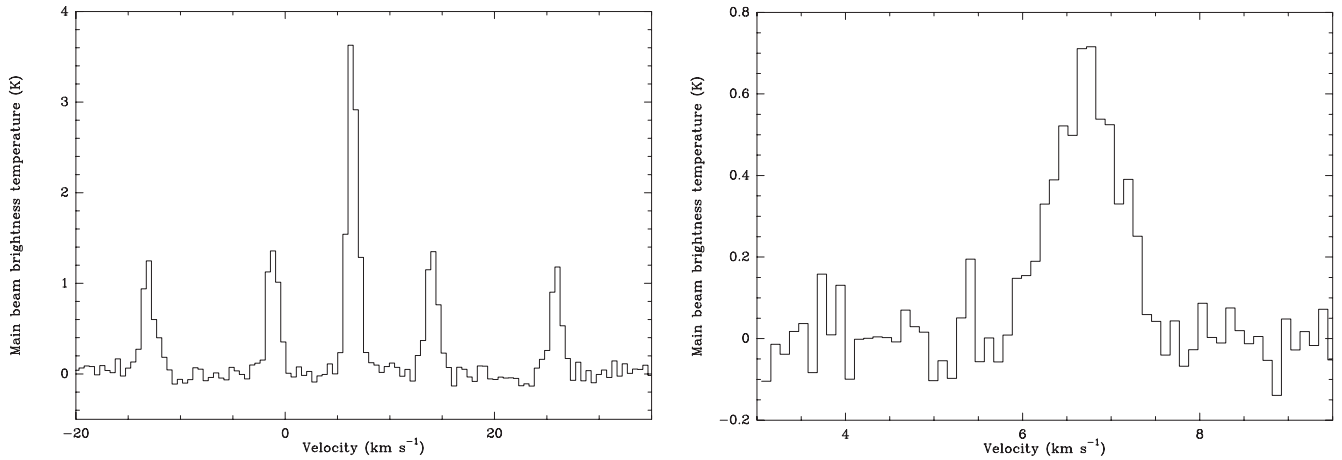


FIG. 8.—Single-dish spectra observed with the Robledo 70 m antenna at the position R.A. = $03^h33^m16^s.34$, decl. = $31°07'51''.1$ (J2000.0). *Left*: NH_3 (1, 1) emission, with rms noise 1 $\sigma = 0.08$ K. *Right*: CCS (2_1–1_0) spectrum, with rms noise 1 $\sigma = 0.13$ K.

An alternative scenario to explain the CCS kinematics is outflowing clumps driven by a wind. If this wind exhibits a Hubble flow–type velocity, which increases with distance from the driving source (as it is observed in other outflows from class 0 protostars; Chandler & Richer 2001), we could explain the velocity pattern by background clumps interacting with and being accelerated by the outflowing material. In order to have redshifted CCS emission at both to the northeast and southwest from the central source, the outflow must lie near the plane of the sky, and the CCS clumps should be associated with the back side of the outflow, both for the southwestern, blueshifted CO lobe and the (as yet) undetected northeastern, redshifted CO lobe.

A way to distinguish between these two models (foreground infalling clumps decelerated by the outflow vs. background outflowing accelerated clumps) is to ascertain whether the motions observed in the CCS clumps can be gravitationally bound. There are two main components in the observed motions: the internal velocity gradients within the clumps and the bulk velocity of the whole clump with respect to the central source. For the first component, the mass M needed to gravitationally bind a cloud of size R with velocity gradient dV/dl is $M = V^2RG^{-1}$, with $V = (dV/dl)R$. This means that the masses needed to bind the internal gradient within each clump are 1.3, 0.3, and 0.4 $M_\odot$ for the SW, NW, and NE clumps, respectively. The masses derived for the clumps (Table 4) are on the same order as those necessary for the clumps to be bound, although we must consider this result carefully due to the very large uncertainties involved in these calculations.

On the other hand, if we consider an average velocity of each CCS clump with respect to that of the ambient cloud and the distance from the infrared source to the center of each clump, the masses needed to bind the motions respectively for the SW, NW, and NE CCS clumps as a whole are 6, 0.4, and 6 $M_\odot$, respectively. The mass of gas contained in a region of radius equal to the distance to the central source would be 13–30 $M_\odot$ for the SW clump, 5–11 $M_\odot$ for the NW clump, and 51–120 $M_\odot$ for the NE clump, depending on whether the values of N_{H_2} were obtained from either averaged values for NH_3 or CCS.

TABLE 4
PHYSICAL PARAMETERS OF THE CLUMPS OBSERVED IN NH_3 AND CCS

Molecule	Clump	I_ν[a] (mJy beam^{-1})	$\int I_\nu\, dv$[a] (mJy beam^{-1} km s^{-1})	N_{mol}[b] (10^{13} cm^{-2})	N_{H_2}[c] (10^{23} cm^{-2})	Sizes[d] (AU × AU)	M_c[e] ($M_\odot$)
NH_3	Mean[f]	170 ± 30	210 ± 30	140 ± 40	1.4 ± 0.4	10700 × 4600	2.1 ± 0.6
CCS	SW1	14.2 ± 2.8	7.5 ± 1.4	3.7 ± 1.7	4.1 ± 1.9	2900 × 2900	1.1 ± 0.5
CCS	SW2	10.5 ± 2.8	6.0 ± 1.4	2.9 ± 1.5	3.2 ± 1.7	5000 × 2900	1.4 ± 0.7
CCS	NW	4.7 ± 2.6	3.4 ± 1.3	1.7 ± 1.1	1.9 ± 1.2	7000 × 2100	0.8 ± 0.5
CCS	NE	9.3 ± 3.9	7.3 ± 2.0	3.6 ± 1.7	4.0 ± 1.9	12600 × 2900	4.4 ± 2.0

NOTE.—All the uncertainties in this table are 2 σ.

[a] Intensity and integrated intensity at the position of the emission peak for each clump (main hyperfine component only for ammonia).

[b] Column density obtained from $N_{mol} = (8\alpha\pi\nu^3/c^3 g_j A_{ji})\{[Q(T_{rot})\int I_\nu\, dv]/[B_\nu(T_{ex}) - B_\nu(T_{bg})]\}\{[\exp(E_j/kT_{rot})]/[\exp(h\nu/kT_{ex}) - 1]\}$ (optically thin approximation), where α is a factor equal to 1 for CCS and equal to $2[1 + \exp(h\nu/kT_{ex})]$ for NH_3, ν is the frequency of the transition, Q is the partition function, $\int I_\nu\, dv$ is the integrated intensity (referred only to the main line in the case of the ammonia), E_j is the energy of the upper state in the case of CCS (1.61 K; Wolkovitch et al. 1997) and the energy of the rotational level whose inversion transition is observed in the case of ammonia (23.4 K; Ho & Townes 1983), T_{rot} is the rotational temperature, g_j is the statistical weight of the upper rotational level in the case of CCS and of the upper sublevel involved in the inversion transition in the case of ammonia, A_{ji} is the Einstein coefficient for the overall transition [1.67 and 4.33×10^{-7} s^{-1} for the NH_3 (1, 1) and CCS (2_1–1_0) transitions, respectively; Ho & Townes 1983; Wolkovitch et al. 1997], and T_{ex} is the excitation temperature. For the CCS molecule we adopted $T_{rot} = T_{ex} = 5$ K (Suzuki et al. 1992). For the NH_3 calculations, we have assumed $T_{rot} = 12$ K, derived by Bachiller & Cernicharo (1984) from single-dish observations. From our single-dish ammonia spectrum (see Fig. 8), we derived an optical depth of $\tau = 0.9 \pm 0.5$, which provides $T_{ex} = 8.8 \pm 2.4$ K. The final N_{NH_3} was obtained by multiplying the optically thin solution by the factor $\tau/(1 - e^{-\tau})$.

[c] Hydrogen column density, obtained assuming a fractional abundance with respect to H_2 of 10^{-8} for NH_3 (Herbst & Klemperer 1973) and 0.9×10^{-10} for CCS (Lai & Crutcher 2000).

[d] FWHM of the clumps. It is an averaged value in the case of ammonia.

[e] Clump mass, derived from N_{H_2} and the half-power area. It is an average value for ammonia clumps.

[f] Average value for the NH_3 clumps.

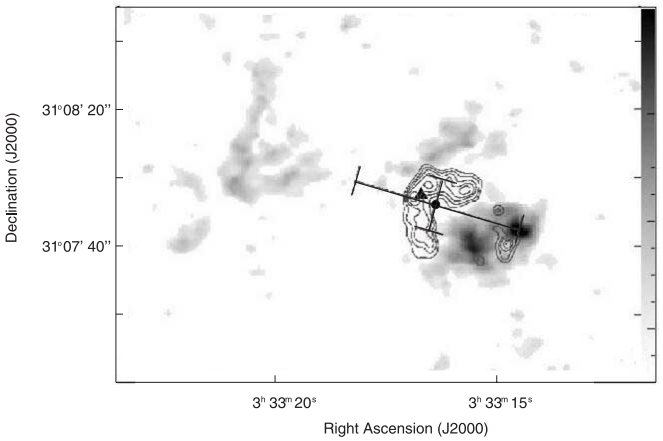


FIG. 9.—Overlay of the CO blueshifted outflow (*contours*; Hirano et al. 1997) and CCS integrated emission (*gray scale*; this paper). The filled circle represents the *IRAS* source with its error position bars. The triangle marks the 2 μm point source. The CCS emission is not corrected for the response of the primary beam.

Therefore, we see that the observed motions in the CCS clumps can be gravitationally bound, a fact that does not allow us to discard either of the alternative models. Regardless of the real geometry and dynamics of the region, it seems that there is an important interaction of the ambient gas with the molecular outflow.

We must point out that the observed CCS clumps may not really be physical entities. These clumps are likely to represent regions of enhanced abundance of CCS (Suzuki et al. 1992; Ohashi et al. 1999). This chemical gradient of CCS is a result of variations in the local conditions of the cloud (Lai et al. 2003). However, our mass estimates to check whether the motions are gravitationally bound are still valid even if the enhanced CCS emission are not physical clumps, given that we are calculating the mass of the region of gas enclosed by the CCS emission. The largest source of uncertainty is the value of the molecular abundance, which is a common problem when deriving column densities using other molecular tracers. In our calculations we consider a fractional abundance of CCS with respect to H_2 of 0.9×10^{-10}, which is the mean value reported by Lai & Crutcher (2000) for this region.

4.4. *Chemical Evolution:* CCS *versus* NH_3

Single-dish observations show that CCS is more abundant in starless, cold, quiescent dark cores (such as L1521B, L1498, TMC-1C, or L1544; Suzuki et al. 1992), while ammonia emission tends to be intense in star-forming regions. These results suggested that CCS is a tracer of early-time chemistry ($t \leq 10^5$ yr), while ammonia is a tracer of more evolved gas (Hirahara et al. 1992; Velusamy et al. 1995; Bergin & Langer 1997).

The abundance ratio N_{NH_3}/N_{CCS} has therefore been proposed by Suzuki et al. (1992) as an indicator of the evolutionary stage of molecular clouds. Our single-dish data provide column densities of $N_{NH_3} \simeq (6 \pm 4) \times 10^{14}$ and $N_{CCS} \simeq (1.70 \pm 0.24) \times 10^{13}$ cm^{-2}. Thus, the ratio N_{NH_3}/N_{CCS} is $\simeq$35, which is significantly lower than the value $\geq$100 found by Suzuki et al. (1992) in most of the star-forming regions in their survey. This relative lack of ammonia, or enhanced CCS, may be an indication of the early evolutionary stage of B1-IRS. However, this result could depend on the particular chemistry of each region, and we must be careful in this interpretation.

In previous single-dish works, a spatial anticorrelation between CCS and ammonia was found, both by comparing detections of those molecules in surveys of sources (Suzuki et al. 1992) and by mapping their emission in the same region (Lai et al. 2003). It is interesting to check whether this anticorrelation still stands when we map a source at high resolution. The overlay of our CCS and ammonia maps (Fig. 7) shows a clear anticorrelation between them throughout the B1-IRS region, except $\simeq$30″ to the north of the ammonia maximum (which coincides with the NE CCS clump), where there is some superposition. This is the first time that this anticorrelation is observed at such a high resolution ($\simeq$5″ = 1750 AU) in a star-forming region, and it illustrates that the chemistry is not only time-dependent, but also exhibits small-scale spatial structure that can seriously affect the interpretation of derived physical and dynamical properties if it is not properly taken into account.

The chemical gradients traced by these molecules may be the result of changing the local conditions. At this moment, most of the theoretical chemical models considering the age and distance to the cloud center include a large number of physical parameters to study the variation of the column density, the distribution, and the fractional abundance of molecules such as CCS and NH_3, among other species. Some of these models include the strength of magnetic fields, the initial chemical composition of the cloud, the probability of molecules sticking to dust grains, the cosmic-ray ionization rate, and the cloud mass (Shematovich et al. 2003); UV photodissociation, cosmic ray–induced photoionization and photodissociation reactions, CO depletion onto grains, and desorption by cosmic rays (Nejad & Wagenblast 1999); or core geometry and view angles (Aikawa et al. 2003). Until now, these chemical studies focused on starless cores and did not consider the effects of a central star, probably because most of the CCS studies have been made toward starless cores (Kuiper et al. 1996; Ohashi et al. 1999; Lai et al. 2003; Shinnaga et al. 2004).

The way in which all these factors and the activity of protostars (in the case of star-forming regions) can modify the classical ion-molecule or radical-neutral pathways of production of molecules such as CCS (Smith 1988; Suzuki et al. 1988; Petrie 1996; Scappini & Codella 1996) needs to be studied in theoretical works to give a better interpretation of our results. The development of models that implement the onset of energetic activity associated with the formation of a star and how this affects the CCS and NH_3 production will be the key to ascertain the evolutionary stage of B1-IRS. Models treating consistently both CCS and NH_3 and considering the effect of young stars could provide more reliable values of the relative abundances and column densities of both molecules as a function of the distance from the source. On the other hand, our data on B1-IRS could be used as a reference work to test the predictions of those calculations in detail. Future comparison with other regions observed with high angular resolution will be vital for understanding the precise meaning of the ratio between the CCS and NH_3 abundances in star-forming regions in terms of chemical evolution.

Moreover, detailed chemical studies in molecular clouds are an important science driver for the development of new interferometers (e.g., the Submillimeter Array [SMA] or the Atacama Large Millimeter Array [ALMA]; see van Dishoeck & Blake 1998; Phillips & Vastel 2003). Our anticorrelation result at a small scale proves that chemical studies is indeed a promising line of research for these new telescopes.

The clumpy distribution of CCS emission detected in B1-IRS has already been observed by other authors in several molecular clouds, such as B335 (Velusamy et al. 1995), L1498 (Kuiper et al. 1996), and TMC-1 (Langer et al. 1995). In the case of B1-IRS, this clumpy distribution was first detected by Lai &

Crutcher (2000) in the CCS $J_N = 3_2-2_1$ transition at 33.8 GHz with the Berkeley-Illinois-Maryland Association (BIMA) interferometer with an angular resolution of $\simeq 30''$. In particular, there seems to be a spatial coincidence between BIMA clumps F and B and our VLA clumps SW and NE, respectively. Moreover, our VLA observations reveal a lack of CCS emission at the position of B1-IRS. This absence of emission has been suggested to be due to a lower abundance of the molecule rather than to a density decrease, since this molecule needs high density to be excited and the density is expected to be higher toward the center (Velusamy et al. 1995). The clumpy distribution could be due to an episodic infall (as suggested by Velusamy et al. [1995] for B335).

Another possibility that is worth considering is that CCS might be locally enhanced in shocked regions. In fact, the observed CCS clumps show kinematical signs of interaction with the outflow, which suggests that the CCS emission could originate from gas affected by the impact of shocks. The outflow could squeeze low-density gas to the higher densities ($\simeq 10^5$ cm^{-3}) needed to produce the CCS and trigger the formation of the molecule. Such low-density gas exists around dense clouds like B1, and the outflow associated with B1-IRS could interact with fresh material around the dense core. Although there is currently no chemical model that includes this kind of phenomena related to star formation, to support the suggested enhancement, observations of other molecules have suggested that their abundance is enhanced in the environment of jets and outflows by shock-induced chemistry, as in the cases of CS (Arce & Sargent 2004), NH_3 (Torrelles et al. 1992, 1993), or HCO^+ (Girart et al. 2000). Theoretical chemical models support those findings (Taylor & Williams 1996; Viti et al. 2002; Wolfire & Koenigl 1993). In particular, for HCO^+ it has been proposed that in some cases its abundance may be increased by a fast outflow impinging on fragments of dense gas (Rawlings et al. 2000), and this type of interaction between an outflow and dense gas is also suggested by our CCS data, although the chemical reactions involved are certainly different.

If this abundance enhancement takes place in short timescales ($\simeq 10^5$ yr), one could expect to find clumps on the order of $5''$ at the distance of B1 (350 pc), considering a typical sound speed of $\simeq 0.1$ km s^{-1}. Therefore, new interferometric observations of CCS in other star-forming regions would be necessary to study these processes.

The association of the central source with water maser emission (which typically lasts for $\simeq 10^5$ yr in star-forming regions; Forster & Caswell 1989) and the existence of CCS, a molecule characteristic of early-time chemistry (Hirahara et al. 1992; Suzuki et al. 1992) confirms the early stage of evolution of B1-IRS. The presence of CCS can be used as a marker of extreme youth among Class 0 protostars (I. de Gregorio-Monsalvo 2005, in preparation). Furthermore, this combination of spatial, kinematic, and dynamical information from CCS and ammonia may be used as a powerful tool to study the processes taking place in the vicinity of very young Class 0 protostars and not just in quiescent cores.

Clearly, further interferometric CCS observations of the environment of other young stellar objects, as well as theoretical chemical models, will be useful to determine whether CCS emission tends to selectively trace regions of interaction of the outflow with its surrounding medium. These studies, combined with high-resolution data of NH_3 and other molecular tracers, will also help to determine the spatial distribution and dynamical evolution of these species.

5. CONCLUSIONS

We have presented high-resolution observations of ammonia, CCS, and water masers toward the Class 0 object B1-IRS (IRAS 03301+3057). Our main conclusions are as follows.

1. There is a 2MASS infrared point source located $\sim 6''$ northeast from the nominal position of the *IRAS* source and at the northeast tip of a blueshifted CO outflow lobe. Fainter infrared emission extending toward the southwest from the point source is also detected.
2. There is a group of water masers associated with the infrared point source. Their elongated distribution (in the northeast-southwest direction) and their unbound motions suggest that these masers are tracing the base of the outflow.
3. The infrared and water maser data suggest that the infrared point source traces the position of the powering source of the mass-loss phenomena in the region and that mass is ejected along the northeast-southwest direction.
4. We detect three clumps of CCS emission surrounding the infrared source, all redshifted with respect to the systemic cloud velocity. They show clear velocity gradients, with less redshifted gas toward the central source. We interpret these gradients in terms of clumps that are strongly interacting with a molecular outflow that lies almost in the plane of the sky.
5. Ammonia emission is weak and extended. It shows a spatial anticorrelation with CCS. Although this kind of anticorrelation is known to be present in other star-forming regions, this is the first time that it has been observed with such a high angular resolution ($\simeq 5''$).
6. The abundance ratio between ammonia and CCS is significantly lower than that found in other star-forming regions. Given the fast disappearance of CCS in star-forming regions, this low ratio might be an indication that B1-IRS is an extremely young stellar object ($\leq 10^5$ yr).
7. We suggest the possibility that CCS abundance is enhanced via shock-induced chemistry. However, theoretical calculations will be needed to confirm this hypothesis.

G. A., J. F. G., I. d. G.-M., and J. M. T. acknowledge support from the Ministry of Science and Technology (MCyT) grant (European Fund of Regional Development [FEDER]) AYA2002-00376 (Spain). G. A. acknowledges support from Junta de Andalucía. I. d. G.-M. acknowledges the support of a Calvo Rodés Fellowship from the Instituto Nacional de Técnica Aeroespacial (INTA). She is also thankful to NRAO for their financial support and to the Array Operations Center (AOC) staff for their hospitality during her stay as a NRAO summer student. We are thankful to Luis Felipe Rodríguez for his useful comments on the manuscript and to María Rosa Zapatero Osorio for her help with the 2MASS data. This paper is partly based on observations taken during "host-country" allocated time at Robledo de Chavela; this time is managed by the Laboratorio de Astrofísica Espacial y Física Fundamental (LAEFF) of INTA, under agreement with the National Aeronautics and Space Administration/Ingeniería y Servicios Aeroespaciales (NASA/INSA). It also makes use of data products from the Two Micron All Sky Survey (2MASS), which is a joint project of the University of Massachusetts and the Infrared Processing and Analysis Center at the California Institute of Technology, funded by NASA and the NSF.

REFERENCES

Aikawa, Y., Ohashi, N., & Herbst, E. 2003, ApJ, 593, 906
André, P., Ward-Thompson, D., & Barsony, M. 1993, ApJ, 406, 122
Arce, H. G., & Sargent, A. I. 2004, ApJ, 612, 342
Bachiller, R., & Cernicharo, J. 1984, A&A, 140, 414
———. 1986, A&A, 166, 283
Bachiller, R., Menten, K. M., & del Río Álvarez, S. 1990, A&A, 236, 461
Bergin, E. A., & Langer, W. D. 1997, ApJ, 486, 316
Briggs, D. 1995, Ph.D. thesis, New Mexico Inst. Mining and Technology
Chandler, C. J., & Richer, J. S. 2001, ApJ, 555, 139
Chandler, C. J., & Sargent, A. I. 1993, ApJ, 414, L29
De Buizer, J. M., Radomski, J. T., Telesco, C. M., & Piña, R. K. 2005, ApJS, 156, 179
Forster, J. R., & Caswell, J. L. 1989, A&A, 213, 339
Furuya, R. S., Kitamura, Y., Wootten, H. A., Claussen, M. J., & Kawabe, R. 2001, ApJ, 559, L143
———. 2003, ApJS, 144, 71
Girart, J. M., Estalella, R., Ho, P. T. P., & Rudolph, A. L. 2000, ApJ, 539, 763
Herbst, E., & Klemperer, W. 1973, ApJ, 185, 505
Hirahara, Y., et al. 1992, ApJ, 394, 539
Hirano, N., Kameya, O., Mikami, H., Saito, S., Umemoto, T., & Yamamoto, S. 1997, ApJ, 478, 631
Ho, P. T. P., & Townes, C. H. 1983, ARA&A, 21, 239
Kuiper, T. B. H., Langer, W. D., & Velusamy, T. 1996, ApJ, 468, 761
Lai, S., & Crutcher, R. M. 2000, ApJS, 128, 271
Lai, S., Velusamy, T., Langer, W. D., & Kuiper, T. B. H. 2003, AJ, 126, 311
Langer, W. D., Velusamy, T., Kuiper, T. B. H., Levin, S., Olsen, E., & Migenes, V. 1995, ApJ, 453, 293
Matthews, B. C., & Wilson, C. D. 2002, ApJ, 574, 822
Menten, K. M., Krügel, E., & Walmsley, C. M. 1983, Mitt. Astron. Ges., 60, 409
Nejad, L. A. M., & Wagenblast, R. 1999, A&A, 350, 204
Ohashi, N., Lee, S. W., Wilner, D. J., & Hayashi, M. 1999, ApJ, 518, L41
Petrie, S. 1996, MNRAS, 281, 666
Phillips, T. G., & Vastel, C. 2003, in SFChem 2002: Chemistry as a Diagnostic of Star Formation, ed. C. L. Curry & M. Fich (Ottawa: NRC Press), 3
Rawlings, J. M. C., Taylor, S. D., & Williams, D. A. 2000, MNRAS, 313, 461
Rodríguez, L. F., Moran, J. M., Gottlieb, E. W., & Ho, P. T. P. 1980, ApJ, 235, 845
Saito, S., Kawaguchi, K., Yamamoto, S., Ohishi, M., Suzuki, H., & Kaifu, N. 1987, ApJ, 317, L115
Scappini, F., & Codella, C. 1996, MNRAS, 282, 587
Shematovich, V. I., Wiebe, D. S., Shustov, B. M., & Li, Z. 2003, ApJ, 588, 894
Shinnaga, H., Ohashi, N., Lee, S., & Moriarty-Schieven, G. H. 2004, ApJ, 601, 962
Smith, I. W. M. 1988, in Rate Coefficients in Astrochemistry, ed. T. J. Millar & D. A. Williams (Dordrecht: Kluwer), 106
Suzuki, H., Ohishi, M., Kaifu, N., Kasuga, T., Ishikawa, S., & Miyaji, T. 1988, Vistas Astron., 31, 459
Suzuki, H., Yamamoto, S., Ohishi, M., Kaifu, N., Ishikawa, S., Hirahara, Y., & Takano, S. 1992, ApJ, 392, 551
Taylor, S. D., & Williams, D. A. 1996, MNRAS, 282, 1343
Terebey, S., Chandler, C. J., & André, P. 1993, ApJ, 414, 759
Torrelles, J. M., Gómez, J. F., Ho, P. T. P., Anglada, G., Rodríguez, L. F., & Cantó, J. 1993, ApJ, 417, 655
Torrelles, J. M., Patel, N. A., Gómez, J. F., & Anglada, G. 2002, in Rev. Mex. AA Ser. Conf., 13, 108
Torrelles, J. M., Rodríguez, L. F., Cantó, J., Anglada, G., Gómez, J. F., Curiel, S., & Ho, P. T. P. 1992, ApJ, 396, L95
van Dishoeck, E. F., & Blake, G. A. 1998, ARA&A, 36, 317
Velusamy, T., Kuiper, T. B. H., & Langer, W. D. 1995, ApJ, 451, L75
Viti, S., Natarajan, S., & Williams, D. A. 2002, MNRAS, 336, 797
Willacy, K., Langer, W. D., & Velusamy, T. 1998, ApJ, 507, L171
Wolfire, M. G., & Koenigl, A. 1993, ApJ, 415, 204
Wolkovitch, D., Langer, W. D., Goldsmith, P. F., & Heyer, M. 1997, ApJ, 477, 241
Yamamoto, S., Mikami, H., Saito, S., Kaifu, N., Ohishi, M., & Kawaguchi, K. 1992, PASJ, 44, 459